P500609.PDF [Page: 3 of 22]

Multiple-scattering lidar equation

Luc R. Bissonnette

A multiple-scattering lidar equation is derived from a phenomenological representation of the scattering processes. The contributions are separated into the unscattered, singly scattered, and multiply scattered illumination of the scattering volume, a single backscattering reflection from that volume, and the unscattered and multiply scattered propagation back to the receiver. The equation is obtained in the form of analytic expressions that explicitly show the signal dependence on the extinction coefficient, the effective particle size, the range, and the receiver field of view. Consistent agreement is found with Monte Carlo calculations and published laboratory measurements. Numerical simulations demonstrate that measurements made at three or more fields of view can be inverted to solve for the extinction coefficient and the effective particle radius. The multiple scatterings taken into account in the proposed equation are the small-angle diffraction scatterings; the wide-angle scatterings caused by refraction and reflection are considered lost, except for one backscattering at an angle close to 180°. Consequently, the equation is applicable to cases in which the projection of the lidar receiver field of view on the cloud is of the order of the angular width of the diffraction peak of the phase function times the penetration depth into the cloud. © 1996 Optical Society of America

Key words: Multiple aerosol scattering, lidar equation, lidar inversion, aerosol lidar.

1. Introduction

Lidars have proved to be powerful tools for the remote sensing of various atmospheric parameters. The most successful applications have relied on single-scattering models of the interaction processes responsible for the detected backscattered radiation from the atmospheric species of interest. However, for cloud measurements, it was quickly realized that multiple-scattering events had to be taken into account. Such studies date back to the early 1970's. For example, Allen and Platt[1] measured multiply scattered lidar returns with a center-blocked field stop, Pal and Carswell[2] showed evidence of multiple-scattering contributions by detection of the cross-polarized component of the received signals, and Sassen and Petrilla[3] made both depolarization and different field-of-view measurements to demonstrate multiple-scattering effects. Recently, Bissonnette and Hutt,[4] Werner *et al.*,[5] and Hutt *et al.*[6] built lidars to make systematic measurements of multiply scattered lidar returns.

The author is with the Defence Research Establishment Valcartier, 2459 Pie-XI Boulevard North, Val-Bélair, Québec G3J 1X5, Canada.

Received 3 May 1995; revised manuscript received 21 December 1995.

0003-6935/96/336449-17$10.00/0

© 1996 Optical Society of America

The early preoccupations were for correcting the multiple-scattering effects, but it was soon discovered[1–3] that recoverable information on the microphysical properties of clouds was contained in the multiple-scattering contributions. It is the purpose of this paper to report on the development of a suitable multiple-scattering lidar equation to recover at least part of this information. Research in this direction was pioneered by Eloranta[7] and Platt.[8] Eloranta developed an analytic model of doubly scattered lidar returns, and Platt introduced a multiplicative factor $\eta < 1$ to reduce the extinction term in the lidar equation. Both approaches are useful for explaining a large number of observed multiple-scattering phenomena, but their predictive capabilities are limited, in the first case by truncation to second scattering order, and in the second case by the lack of a suitable theoretical formulation for factor η. However, a great deal of progress has been accomplished over the past 10–15 years on more sophisticated models. Various approaches have been pursued; they include approximations to the radiative transfer equation, Monte Carlo calculations, stochastic models, and analytical extensions of the Mie theory. A complete review of this subject is beyond the scope of this paper, but Ref. 9 gives a good picture of the diversity and complexity of the models by grouping together in an intercomparison study a number of theoretical simulations of multiply scat-

tered lidar returns. Numerous relevant references are also cited in that article.

The models of Ref. 9 are complex for the inverse problem, i.e., the determination of microphysical properties of clouds from measured lidar returns. As a possible candidate to achieve inversion, a simplified formulation of a multiple-scattering lidar equation is proposed here. The equation is explicitly dependent on the extinction coefficient, $\alpha(z)$, and effective diameter, $d(z)$, of the aerosol particles for each range z of the lidar signal. Hence, inverse solutions for $\alpha(z)$ and $d(z)$ can be obtained through straightforward numerical algorithms. Such an inversion method based on an early version of the model of this paper was tested in two field experiments, in which the cloud microphysical parameters were independently measured with *in situ* sensors. The results are reported in Ref. 10, where it is shown that the profiles of the extinction coefficients, the effective particle radius, and liquid water content can be determined with good accuracy.

The model derivation is outlined in Section 2. Section 3 compares predictions with Monte Carlo calculations and laboratory simulation data. The inverse problem is discussed in Section 4.

2. Lidar Equation

I describe the derivation of a multiple-scattering lidar equation. The main objective is to arrive at a formulation amenable to inversion. Restriction is made to aerosols having a large size parameter $\pi d/\lambda$, where d is the effective particle diameter and λ is the lidar wavelength. With this condition we assume that the multiply scattered photons collected within the small fields of view of practical lidar receivers originate exclusively from the forward diffraction peak of the scattering phase function; the remaining wide-angle geometric scatterings are considered lost, except for one backscattering near 180°. Furthermore, size parameter $\pi d/\lambda$ is assumed to be large enough for the diffraction scatterings to make up half of the extinction coefficient. This constitutes the main approximation of the proposed model; it is justified for ground-based cloud measurements at visible or near-infrared wavelengths as long as the fields of view are kept small. The results are analytic expressions for the multiply scattered contributions to the lidar signals that explicitly show the dependence on the aerosol extinction coefficient and effective particle size. The inverse problem is thus made relatively straightforward.

The assumption of large size parameters is not as restrictive as it might appear, because for size parameters of the order of one or smaller, the scattering is so widely spread that hardly any multiple scatterings can be detected within the small fields of view of practical lidar receivers.

The model is phenomenological. The various contributions are treated separately to take advantage of the fact that some of the mechanisms, and at small optical depths the most significant ones, can be modeled almost exactly. This is the case for the single and double scatterings. As for the more complicated situation of multiple forward scatterings, a simple *ad hoc* model is adopted; it is based on the assumption of a diffusion mechanism[11,12] for modeling the lateral spreading, and the separation of the resulting radiance into the product of two functions that represent its spatial and angular dependences, respectively. The derivation details are given below.

The lidar equation must describe the following process. A short laser pulse illuminates through direct and forward scattered radiation the ambient aerosol particles. A receiver collocated with the laser captures within a given field of view the radiation backscattered by the aerosol as a function of the time T following the emission of the laser pulse. The signal at T is thus the radiation reflected from a distance $z = cT/2$, where c is the speed of light. The range thickness over which the reflection takes place, i.e., the lidar spatial resolution, is $ct/2$, where t is the pulse duration; this neglects the spreading caused by multiple scattering. The proposed model follows this simple phenomenological description. We successively obtain expressions for the illuminating radiance at z, convolve these with the angular backscattering function, and propagate the reflected radiation back to the receiver. What differs from the conventional single-scattering model is that the multiple scatterings that contribute to the illumination of the particles in the forward direction and that redirect photons into the receiver field of view in the backward direction are taken into account. However, all contributing scatterings are assumed to take place in the near-forward direction, except for one backscattering at an angle close to 180°.

A. Illuminating Radiance

The illuminating radiance at range z is separated into three components: (a) the unscattered beam I_{un}; (b) the singly forward-scattered radiation originating from the unscattered incident narrow laser pulse I_{ss}; and (c) the multiply scattered photons from all off-axis positions I_{mm}. The radiance is defined here per unit of solid angle measured from the lidar position. Transformation to conventional radiance requires division by the range squared. Appendix A lists the symbols and definitions most frequently used in this paper.

The expression for the unscattered laser pulse is straightforward. It is given by

$$I_{un}(z, \beta, \vartheta) = \frac{P_0 \exp(-\beta^2/\beta_0^2)}{\pi\beta_0^2} \exp[-\tau(z)]\delta(\vartheta - \beta), \tag{1}$$

where β is the angle with respect to the lidar axis measured from the lidar position, ϑ defines the angular distribution of I_{un} at (z, β),

$$\tau(z) = \int_0^z \alpha(z')dz' \tag{2}$$

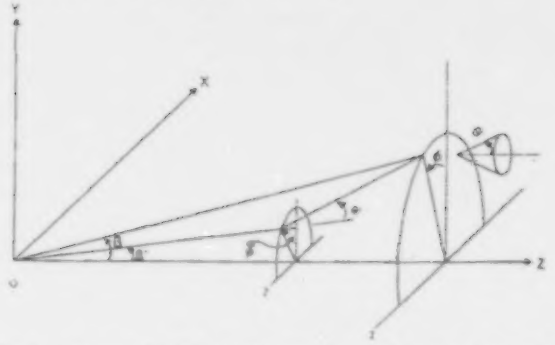

Fig. 1. Diagram illustrating the geometry used for calculating the singly forward-scattered illuminating radiance.

is the optical depth, α is the extinction coefficient, P_0 and β_0 are, respectively, the average power and divergence of the laser pulse, and δ is the Kronecker delta normalized such that $\int d^2\vartheta\delta(\vartheta) = 1$. The profile of the laser pulse was taken as Gaussian, and it is further assumed that $\beta_0 \ll 1$, in accordance with common practice in lidar design.

The singly forward-scattered illuminating radiance I_{ss} is the sum of all first scatterings stripped from the unscattered laser pulse and ending up in plane z. Figure 1 illustrates the geometry and gives a schematic definition of the relevant variables. With reference to Fig. 1, I_{ss} is given by

$$I_{ss}(z, \beta, \vartheta) = \int_0^{\infty}\int_0^{2\pi}\int_z^{\bar{z}}\left\{\exp[-\tau(z')] \times \frac{P_0 \exp(-\beta'^2/\beta_0^2)}{\pi\beta_0^2}\beta' d\beta' d\phi'\right\} \times [\alpha_s(z')p(z', \theta')dz'] \times \left[\frac{z^2\cos^2\theta'\beta d\beta d\phi}{(z-z')^2}\right]\left(\frac{1}{d\phi\beta d\beta}\right) \times \{\exp[-\tau(z) + \tau(z')]\}\delta(\vartheta - \theta'), \quad (3)$$

where the first group of terms within braces is the incident unscattered power through solid angle $\beta' d\beta' d\phi'$, the first group within brackets is the fraction of the incident radiation scattered in direction θ' per unit of solid angle, the second group within brackets is the solid angle subtended at z' by infinitesimal area $z^2\beta d\beta d\phi$ at (z, β, ϕ) through which the radiation is scattered, $(1/d\phi\beta d\beta)$ is the inverse of the element of solid angle measured from the lidar position used to normalize I_{ss} to a unit of solid angle, the second group within braces gives the losses for propagation from z' to z, and finally $\delta(\vartheta - \theta')$ is the angular distribution at (z, β) of the radiation scattered at z' from the unscattered laser pulse.

In these expressions, $\bar{z}$ is the distance to the boundary of the cloud, α_s is the scattering coefficient, p is the angular scattering phase function normalized such that $\int d^2\theta p(z, \theta) = 1$, and θ' is given by

$$\theta'^2 = \frac{z^2}{(z-z')^2}[\beta^2 + \beta'^2 - 2\beta\beta'\cos(\phi - \phi')] + \cdots, \quad (4)$$

which was obtained by expanding $\cos\theta'$ determined by the scalar product of the unit vectors along line segments $(0, 0, 0) - (z', \beta', \phi')$ and $(z', \beta', \phi') - (z, \beta, \phi)$. It is assumed in Eqs. (3) and (4) and in all the following derivation steps that all angles measured from the lidar axis are sufficiently small to allow the sine and tangent functions to be replaced by the angle itself, and the cosine functions to be replaced by one.

Rearranging the terms in Eq. (3), for radiance I_{ss} we find that

$$I_{ss}(z, \beta, \vartheta) = \int_z^{\bar{z}} dz' \int_0^{2\pi} d\phi' \times \int_0^{\infty}\beta' d\beta' \frac{P_0\exp(-\beta'^2/\beta_0^2)}{\pi\beta_0^2} \times \exp[-\tau(z)]\alpha_s(z')p(z', \theta') \times \frac{z^2}{(z-z')^2}\delta(\vartheta - \theta'). \quad (5)$$

As stated above, one basic assumption of the proposed model is that the aerosol particles are sufficiently large compared with the wavelength to give rise to a phase function characterized by a strong forward peak. Under this condition, the forward peak is due to diffraction and is given by the well-known Airy function for a single particle size. For polydisperse aerosols, the individual Airy functions are smoothed by the particle-size distribution. To ease the mathematics, we approximate the resulting peak function by a Gaussian, which we write as follows:

$$p(z, \theta) = \frac{A_2}{\omega(z)\pi}y^2(z)\exp[-A_1^2y^2(z)\theta^2], \quad (6)$$

where

$$y(z) = \pi d(z)/\lambda \quad (7)$$

is the size parameter written in terms of effective particle diameter d, defined as the ratio of the third to the second moment of the particle size distribution, $\omega = \alpha_s/\alpha$ is the single-scattering albedo, and A_1 and A_2 are empirical constants. We divide Eq. (6) by the albedo because the diffraction contributions, being independent of absorption, scale with the extinction coefficient and not with the scattering coefficient used to normalize the phase function. Here A_1 and A_2 are not part of the inversion solution; they are constants to be determined only once. How they are determined is discussed below. Size parameter $y(z)$, or particle diameter $d(z)$, is an unknown function of both range z and the time of the emission of the lidar pulse; it is part of the solutions. As Eq. (6) shows,

$y(z)$ characterizes the width and strength of the phase function peak. In what follows, let us use Eq. (6) to represent the phase function and thus consider as losses all other wide-angle scatterings.

We assume for the moment that $\beta'^2 \gg \beta_0^2$ and $\beta_0^2 \ll 1$. Because $\beta' \sim \beta_0$, from Eq. (4) we thus have

$$\theta'^2 \simeq \frac{\beta^2 z^2}{(z - z')^2}. \tag{8}$$

Substituting this expression for θ' and Eq. (6) for p in Eq. (5), we find, after performing the integrations over ϕ' and β', that

$$I_{ss}(z, \beta, \vartheta) = \frac{A_2}{\pi} P_0 \exp[-\tau(z)] \int_z^s dz' \frac{\alpha_s(z')}{\omega(z')} y^3(z') \times \frac{z^2}{(z - z')^2} \exp\left[-\frac{A_1^2 y^2(z') z^2 \beta^2}{(z - z')^3}\right] \times \delta\left(\vartheta - \frac{z}{z - z'}\beta\right). \tag{9}$$

Because of expression $z^2/(z - z')^2$, the z' integration of Eq. (9) is weighted heavily at the value $z'_{peak} \simeq z[1 - A_1 y(z)\beta]$. This allows us to simplify Eq. (9) as follows. First, we can set $z' = z'_{peak}$ in the slowly varying functions of the integrand, including the argument of the δ function, and then pull these terms out from under the integral sign. The result is

$$I_{ss}(z, \beta, \vartheta) = \frac{A_2}{\pi} P_0 \exp[-\tau(z)] \alpha(z'_{peak}) y^3(z'_{peak}) \times \int_z^s dz' \frac{z^2}{(z - z')^2} \times \exp\left[-\frac{A_1^2 y^2(z') z^2 \beta^2}{(z - z')^2}\right] \times \delta\left[\vartheta - \frac{\beta}{A_1 y(z'_{peak})\beta}\right], \tag{10}$$

where $\alpha(z'_{peak})$ has been substituted for $\alpha_s(z'_{peak})/\omega(z'_{peak})$. Performing the z' integration, we find

$$I_{ss}(z, \beta, \vartheta) = \frac{1}{2\pi} \frac{A_2}{A_1} P_0 \exp(-\tau(z)] z \alpha' y' \frac{\sqrt{\pi}}{\beta} \times [1 - \Phi(A_1 y' C\beta)] \delta\left(\vartheta - \frac{\beta}{A_1 y' \beta}\right), \tag{11}$$

where α' and y' stand for $\alpha(z'_{peak})$ and $y(z'_{peak})$, respectively,

$$C = z/(z - \bar{z}), \tag{12}$$

and Φ is the error function defined by

$$\Phi(v) = \frac{2}{\sqrt{\pi}} \int_0^v \exp(-t^2) dt. \tag{13}$$

To complete the model of the illuminating radiance, we need to express the contribution of the multiple forward scatterings, i.e., $I_{mm}(z, \beta, \vartheta)$. Here I_{mm} is made up of the radiation scattered off the laser pulse that reaches plane z after at least one additional off-axis scattering. This is too complex to be formulated into a manageable analytic expression by following the individual scattering events, as we have done for I_{ss}. A more global description is necessary even if we need to sacrifice precision. Accordingly, the following *ad hoc* model is proposed. Because I_{mm} originates from a tightly collimated laser pulse and the subsequent diffraction scatterings are concentrated in the near-forward direction as a result of assumed condition $1/A_1^2 y^2 \ll 1$, its behavior remains rather beamlike. This suggests a diffusion mechanism to represent the spreading of I_{mm}. Finally, we assume that the spatial and angular dependences of I_{mm} are separable into the product of two functions $M_{mm}(z, \beta)$ and $R_{mm}(\vartheta)$ as follows:

$$I_{mm}(z, \beta, \vartheta) = M_{mm}(z, \beta) R_{mm}(\vartheta). \tag{14}$$

This is an intuitive model that is based on a similarity to turbulent transport processes successfully described by diffusion.

The diffusion model requires first the specification of a diffusion coefficient. The diffusion coefficient is proportional to the mean free path between the random events giving rise to the transport of the average property of interest, here $M_{mm}(z, \beta)$, times the number of these events; it has the units of length. For the mean free path, let us choose expression $2(z - z')/[\tau(z) - \tau(z')]$, which satisfies the following desirable properties: it is equal to mean free path $2\omega/\alpha_s = 2/\alpha$ in homogeneous media; it becomes proportional to the propagation distance where the scattered radiation reaches into clear air; and it has history through optical depth τ. The factor of 2 is used in the expression for the mean free path because we are counting only the scatterings that occur within the diffraction forward peak. Finally, the number of contributing scattering events between z' and z is assumed to be given by $(\exp\{[\tau(z) - \tau(z')]/2\} - 1)$. Hence, postulated diffusion coefficient $D(z, z')$ at z for radiation first scattered at z' is

$$D(z, z') = \gamma \frac{2}{A_1 y(z)} \frac{(\exp\{[\tau(z) - \tau(z')]/2\} - 1)}{[\tau(z) - \tau(z')]} (z - z'), \tag{15}$$

where diffraction scattering angle $1/A_1 y$ is used for projection of the mean free path in the transverse plane because we are interested in lateral diffusion, and γ is the proportionality constant set equal to 0.08 as in the model described in Refs. 11 and 12. The integral of the diffusion coefficient gives the square of the average distance from the beam axis to which the scattered photons have migrated. We represent this distance in angular coordinates by $\theta_{mm}(z, z')$, which physically is the width of the beam of radiation first scattered at z' and multiply forward scattered to z. Here $\theta_{mm}^2(z, z')$ is calculated by integrating $D(z, z')$

P500609.PDF [Page: 7 of 22]

over z and dividing through by z^2, i.e.,

$$\theta_{mm}^2(z, z') = \frac{1}{z^2}\left[\beta_0^2 z'^2 + \frac{2\gamma}{A_1} \times \int_{z'}^{z} \frac{(\exp\{[\tau(z'') - \tau(z')]/2\} - 1)}{y(z'')[\tau(z'') - \tau(z')]} \times (z'' - z')dz''\right], \quad (16)$$

where $\beta_0 z'$ is the initial size, i.e., the size of the source beam. Now that we have scale θ_{mm}, we need to assume a profile function for the diffuse beam. By analogy with the I_{ss} term, we postulate a function of the form

$$F \sim \frac{1}{\beta^{1/n}}[1 - \Phi(\beta/\theta_{mm})], \quad (17)$$

where n is the scattering order for propagation between z' and z, i.e.,

$$n = 1 + [\tau(z) - \tau(z')]/2. \quad (18)$$

Division by 2 is used to be consistent with the assumption that the diffraction scatterings are the only contributors. Approximation (17) satisfies the limiting cases of a dependence in $1/\beta$ for $n = 1$ and $\beta \to 0$ as found with I_{ss}, and a uniform profile close to the axis for large n. Normalizing to unity the solid-angle integral of Eq. (17), we find

$$F = \frac{K(z, z')}{\theta_{mm}^2}\left(\frac{\theta_{mm}}{\beta}\right)^{1/n}\{1 - \Phi[\beta/\theta_{mm}(z, z')]\}, \quad (19)$$

where

$$K(z, z') = \frac{2n - 1}{2n}\frac{1}{\sqrt{\pi}\Gamma[(3n - 1)/2n]}, \quad (20)$$

and Γ is the gamma function. Both K and θ_{mm} are functions of z and z'. Introducing the strength and attenuation of all z' contributions and summing over all z', for $M_{mm}(z, \beta)$ we obtain

$$M_{mm}(z, \beta) = \int_z^z dz' P_0 \exp[-\tau(z')]\frac{\alpha(z')}{2}\frac{K}{\theta_{mm}^2}\left(\frac{\theta_{mm}}{\beta}\right)^{1/n} \times [1 - \Phi(\beta/\theta_{mm})](\exp\{-[\tau(z) - \tau(z')]/2\} - \exp[-\tau(z) + \tau(z')]), \quad (21)$$

where $P_0 \exp[-\tau(z')]\alpha(z')dz'/2$ is the radiation scattered by particle diffraction from the unscattered beam, $\exp\{-[\tau(z) - \tau(z')]/2\}$ gives the losses from z' to z by absorption and wide-angle scatterings, and fraction $\exp[-\tau(z) + \tau(z')]$ is removed because it has already been taken into account in $I_{ss}(z, \beta, \vartheta)$.

The angular distribution $R_{mm}(\vartheta)$ of I_{mm} is assumed to be proportional to the convoluted phase function resulting from the multiple forward scatterings, i.e., a function of the form

$$R_{mm}(\vartheta) = \frac{1}{\pi\theta_{pf}^2}\exp(-\vartheta^2/\theta_{pf}^2). \quad (22)$$

The Gaussian shape follows from the assumed shape of the single-scattering phase function, i.e., Eq. (6), and width θ_{pf} starts off equal to the phase-function peak and increases with the number of subsequent scatterings according to the *ad hoc* model

$$\theta_{pf}^2(z) = \frac{1}{A_1^2 y^2(z)} + \int_z^z \frac{dz'\alpha(z')/2}{A_1^2 y^2(z')}. \quad (23)$$

Substituting Eqs. (21) and (22) into Eq. (14), for $I_{mm}(z, \beta, \vartheta)$ we obtain

$$I_{mm}(z, \beta, \vartheta) = \int_z^z dz' \frac{\alpha(z')}{2} P_0 \exp[-\tau(z)] \times (\exp\{[\tau(z) - \tau(z')]/2\} - 1) \times \frac{K}{\theta_{mm}^2}\left(\frac{\theta_{mm}}{\beta}\right)^{1/n}[1 - \Phi(\beta/\theta_{mm})] \times \frac{1}{\pi\theta_{pf}^2(z)}\exp[-\vartheta^2/\theta_{pf}^2(z)]. \quad (24)$$

The proposed model for $I_{mm}(z, \beta, \vartheta)$ involves a fair deal of empiricism. The precision of Eq. (24) is difficult to ascertain *a priori*, but it has the merit of summarizing into a simple analytic expression the global effect of intricate multiple forward scatterings. Validation will depend on *a posteriori* comparisons with measurements or calculations derived from more sophisticated and exact multiple-scattering models.

The sum of Eqs. (1), (11), and (24) constitutes the proposed model for the illuminating radiance at z that results from the direct and forward-scattered laser pulse radiation. It is applicable to aerosols characterized by a predominant forward peak of their single-scattering phase function and to low-divergence laser pulses.

B. Backscatter

The backward propagation over the return path of the reflected radiation is separated into two contributions: unscattered and multiply scattered. Hence, power $P(z, \theta)$ received from range z within a field of view θ is modeled by the sum of two terms:

$$P(z, \theta) = P_{un\,tot}(z, \theta) + P_{ms\,tot}(z, \theta), \quad (25)$$

where the first group of letters in the subscripts refers to the return propagation path, and the second group refers to the forward illumination path. Subscript un stands for unscattered, ms stands for multiply scattered, and tot stands for total or the sum of the unscattered, singly scattered, and multiply scattered contributions.

P500609.PDF [Page: 8 of 22]

The unscattered return, $P_{\text{un tot}}$, is given by

$$P_{\text{un tot}}(z, \theta) = P_{\text{un un}}(z, \theta) + P_{\text{un ss}}(z, \theta) + P_{\text{un mm}}(z, \theta)$$
$$= 2\pi \int_0^{\theta} \beta d\beta \int_0^{2\pi} d\phi \int_0^{\infty} \vartheta d\vartheta \, [I_{\text{un}}(z, \beta, \vartheta) + I_{\text{ss}}(z, \beta, \vartheta) + I_{\text{mm}}(z, \beta, \vartheta)]\alpha_s(z) \times p(z, \pi - |\beta - \vartheta|) \frac{ct}{2} \frac{A}{z^2} \exp[-\tau(z)], \quad (26)$$

where A is the aperture area of the receiver and

$$|\beta - \vartheta| = [\beta^2 + \vartheta^2 - 2\beta\vartheta \cos(\phi - \varphi)]^{1/2}. \quad (27)$$

Summation is over all angles ϑ of the illuminating radiance and over transverse coordinates β to field of view θ.

Equation (26) depends on phase function p near the backscatter angle of π. For the time being, we have no model of the phase function in that region as we did in the forward direction with Eq. (6). For the direct problem, this is not an issue because p is given. In what follows, let us assume an unspecified p and work out approximations that are intended for the inverse problem. It will of course be possible to revisit these approximations if a satisfactory model of $p(z, \pi - \beta)$ becomes available.

In the case of I_{un}, we have for the backscatter function, after substitution of Eq. (1) in Eq. (26) and integration over ϑ, the following expression:

$$\int_0^{2\pi} d\varphi \int_0^{\infty} \vartheta d\vartheta \delta(\vartheta - \beta) p(z, \pi - |\beta - \vartheta|) = p(z, \pi), \quad (28)$$

which is exact. In the case of I_{ss}, we obtain from Eq. (11) in Eq. (26)

$$\int_0^{2\pi} d\varphi \int_0^{\infty} \vartheta d\vartheta p(z, \pi - |\beta - \vartheta|) \times \delta\left(\vartheta - \frac{\beta}{A_1 y' \beta}\right) = p(z, \pi - |\beta - 1/A_1 y'|). \quad (29)$$

Similarly, we find in the case of I_{mm}

$$\int_0^{2\pi} d\varphi \int_0^{\infty} \vartheta d\vartheta p(z, \pi - |\beta - \vartheta|) \frac{1}{\pi \theta_{\text{pf}}^2} \times \exp(-\vartheta^2/\theta_{\text{pf}}^2) = \langle p(z, \pi - \beta) \rangle_{\theta_{\text{pf}}}, \quad (30)$$

where $\langle p(z, \pi - \beta) \rangle_{\theta_{\text{pf}}}$ is the average value of the backward phase function about angle $\pi - \beta$ for angular fluctuations of standard deviation equal to θ_{pf}, as explicitly defined in Eq. (30), $\langle p(z, \pi - \beta) \rangle_{\theta_{\text{pf}}}$ is given by the convolution of the phase function with a Gaussian of width θ_{pf}.

Substituting Eqs. (1), (11), and (24) for I_{un}, I_{ss}, and I_{mm} in Eq. (26) and using Eqs. (28)–(30), we find

$$P_{\text{un tot}}(z, \theta) = P_{\text{ss}}(z) \left[1 + \frac{A_2}{A_1} \int_0^{\theta} \times \beta d\beta \frac{p(z, \pi - |\beta - 1/A_1 y'|)}{p(z, \pi)} \times z\alpha' y' \frac{\sqrt{\pi}}{\beta} [1 - \Phi(A_1 y' C\beta)] + 2\pi \int_0^{\theta} \beta d\beta \int_z^{z} dz' \frac{K}{\theta_{\text{mm}}^2} \left(\frac{\theta_{\text{mm}}}{\beta} \right)^{1/n} \times [1 - \Phi(\beta/\theta_{\text{mm}})] \frac{\langle p(z, \pi - \beta) \rangle \theta_{\text{pf}}}{p(z, \pi)} \frac{\alpha(z')}{2} \times (\exp\{[\tau(z) - \tau(z')]/2\} - 1) \right], \quad (31)$$

where P_{ss} is the conventional single-scattering lidar equation given by

$$P_{\text{ss}}(z) = P_0 \frac{A}{z^2} \frac{ct}{2} \alpha_s(z) p(z, \pi) \exp[-2\tau(z)]. \quad (32)$$

Symbols α' and y' in the second term of Eq. (31) represent functions $\alpha(z')$ and $y(z')$ evaluated at $z' = z'_{\text{peak}} = z(1 - A_1 y\beta)$. We are interested in a field-of-view domain where θ is much less than $1/A_1 y$, i.e., a domain where $P(z, \theta)$ is rapidly changing with θ. This is necessary to have a good sensitivity for extinction coefficient α and size parameter y. Under this condition, $\beta < \theta \ll 1/A_1 y$ and we have $z'_{\text{peak}} \simeq z$. We can thus approximate

$$y' = y(z'_{\text{peak}}) \simeq y(z) = y, \quad (33)$$

$$z\alpha' = z\alpha(z'_{\text{peak}}) \simeq z\alpha(z) = x, \quad (34)$$

where x and y are independent of β. Variables x and y are the two unknowns for which we eventually want to solve; they are nondimensional forms of the extinction coefficient and the effective particle diameter of the aerosol, respectively.

Next, we define

$$\delta_1(z, \theta) = \frac{1}{p(z, \pi)} \times \frac{\int_0^{\theta} d\beta p(z, \pi - |\beta - 1/A_1 y|)[1 - \Phi(A_1 y C\beta)]}{\int_0^{\theta} d\beta [1 - \Phi(A_1 y C\beta)]}, \quad (35)$$

P500609.PDF [Page: 9 of 22]

$$\delta_2(z,\theta)=\frac{1}{p(z,\pi)}\left[\int_0^{\theta}\beta d\beta\langle p(z,\pi-\beta)\rangle_{\theta_{pf}}\times\int_z^{z}dz'\,\frac{K}{\theta_{mm}^{\,2}}\left(\frac{\theta_{mm}}{\beta}\right)^{1/n}[1-\Phi(\beta/\theta_{mm})]\times\frac{\alpha(z')}{2}(\exp\{[\tau(z)-\tau(z')]/2\}-1)\right]\times\left[\int_0^{\theta}\beta d\beta\int_z^{z}dz'\,\frac{K}{\theta_{mm}^{\,2}}\left(\frac{\theta_{mm}}{\beta}\right)^{1/n}\times[1-\Phi(\beta/\theta_{mm})]\frac{\alpha(z')}{2}\times(\exp\{[\tau(z)-\tau(z')]/2\}-1)\right]^{-1}. \quad (36)$$

Functions δ_1 and δ_2 are averages of the normalized backward phase function over an angular range of the order of $1/A_1y$ about π. They are unknown *a priori* unless $p(z, \pi - \beta)$ is given, as is the case in the direct problem. However, for many practical cases, δ_1 and δ_2 are expected to be weak functions of θ and should not differ from unity by more than 20–30%. In other words, the expected errors associated with the uncertainties on δ_1 and δ_2 are estimated at 20–30%.

Substituting Eqs. (33)–(36) into Eq. (31) and performing the β integrations where possible, we obtain

$$P_{un\,tot}(z,\theta)=P_{ss}(z)\left[1+\frac{A_2}{A_1}\delta_1 xy\sqrt{\pi}\times\left[\theta-\theta\Phi(A_1yC\theta)+\frac{1-\exp(-A_1^{\,2}y^2C^2\theta^2)}{A_1yC\sqrt{\pi}}\right]+\delta_2\int_z^{z}dz'\,\frac{\alpha(z')}{2}(\exp\{[\tau(z)-\tau(z')]/2\}-1)\times 2\pi\int_0^{\theta}\beta d\beta\,\frac{K}{\theta_{mm}^{\,2}}\left(\frac{\theta_{mm}}{\beta}\right)^{1/n}\times[1-\Phi(\beta/\theta_{mm})]\right]. \quad (37)$$

Equation (37) was derived by integrating, among other functions, Eq. (11) over β from 0 to θ. However, Eq. (11) is not valid for β of the order of the beam divergence β_0, and hence, Eq. (37) requires corrections. Actually, Eq. (37) is exact in the limit $\beta_0 = 0$. For $\beta_0 \neq 0$, there is a lag in the growth rate of $P_{un\,ss}(z, \theta)$ with respect to θ, for θ of the order of β_0. This means that for $\theta^2 \gg \beta_0^{\,2}$, i.e., in the intended range of applicability of Eq. (37) the true $P_{un\,ss}(z, \theta)$ is shifted downward by a constant value. This constant is determined in Appendix B. The result is

$$P_{un\,tot}(z,\theta)=P_{ss}(z)\left[1-\frac{A_2}{A_1}\delta_1^{\,2}xy\beta_0\div\left[1-\frac{2}{\pi}\tan^{-1}(A_1yC\beta_0)\right]+\frac{A_2}{A_1}\delta_1 xy\sqrt{\pi}\left[\theta-\theta\Phi(A_1yC\theta)+\frac{1-\exp(-A_1^{\,2}y^2C^2\theta^2)}{A_1yC\sqrt{\pi}}\right]+\delta_2\int_z^{z}dz'\,\frac{\alpha(z')}{2}(\exp\{[\tau(z)-\tau(z')]/2\}-1)2\pi\int_0^{\theta}\beta d\beta\,\frac{K}{\theta_{mm}^{\,2}}\left(\frac{\theta_{mm}}{\beta}\right)^{1/n}\times[1-\Phi(\beta/\theta_{mm})]\right]. \quad (38)$$

Equation (38) gives the lidar contributions caused by the unscattered backward return. Referring back to Eq. (25), we find that this leaves the evaluation of the contributions caused by the multiple forward scatterings in the backward direction, i.e., $P_{ms\,tot}$. This is expressed schematically as follows:

$$P_{ms\,tot}=P_{ms\,un}+P_{ms\,ms}, \quad (39)$$

where $P_{ms\,un}$ stands for multiply scattered backward and unscattered forward, and $P_{ms\,ms}$ stands for multiply scattered, both backward and forward.

The first term in Eq. (39), i.e., $P_{ms\,un}$, models the contribution resulting from the unscattered illumination of the backscattering volume followed by multiple forward scatterings in the backward direction. If we represent this by a photon trajectory, we have a straight line coincident with the lidar axis from zero to range z and a series of connected line segments from z to zero, with the last segment crossing the origin zero at some angle θ with the lidar axis. Conceptually, we can perform a rigid rotation of the polygon described by the photon trajectory to bring the last segment coincident with the lidar axis. Because the direction of flight of photons is reversible, and because it was implicitly assumed that the medium is laterally homogeneous over an angular range compatible with the receiver field of view, it follows that for each photon trajectory having no scatterings in the forward direction and multiple scatterings in the backward direction, there is a completely equivalent trajectory with the order of scatterings reversed. Therefore, we have

$$P_{ms\,un}(z,\theta)=P_{un\,ms}(z,\theta), \quad (40)$$

where $P_{\text{un ms}}$ has already been modeled in Eq. (38). Appendix C gives a mathematical demonstration for the special case of $P_{\text{ss un}} = P_{\text{un ss}}$.

Finally, with $P_{\text{ms un}}$ determined by Eq. (40), there remains to model term $P_{\text{ms ms}}$. The situation of the multiple scatterings in the backward direction is quite different from that of the forward propagating I_{mm} that was treated in Subsection 2.A. The radiation backscattered from range z originates from a small scattering volume at z instead of a longitudinally distributed source along a thin tightly collimated beam, as was the case for I_{mm}, and the angular scattering is generally much broader at π than at zero. Hence, the lateral diffusion model that was used to describe the beamlike behavior of I_{mm} is not applicable here. Of course, the microscopic diffusion processes that were assumed for I_{mm} also take place in the backward direction, but the resulting macroscopic effect of laterally spreading the radiation is negligible because the gradient of the average radiance perpendicular to the direction of propagation is small.

A mathematical description of $P_{\text{ms ms}}$ can be written as follows:

$$
\begin{aligned}
P_{\text{ms ms}}(z, \theta) = \frac{A}{z^2}\frac{ct}{2}\alpha_s(z)p(z, \pi)\{&\exp[-\tau(z)/2] \\
&- \exp[-\tau(z)]\}\int_0^\infty d^2\boldsymbol{\beta}\int_0^\infty d^2\boldsymbol{\vartheta} \\
&\times\left[\sum_N\prod_{i=1}^N\int_0^{\Delta_i} d^2\boldsymbol{\theta}_i\int_{z_{i-1}}^{z} dz_i\right. \\
&\left.\times\,\Omega_i(z_i, z_{i+1}, \boldsymbol{\theta}_i, \boldsymbol{\theta}_{i+1})p(z_i, \Theta_i)\alpha_s(z_i)\right] \\
&\times\frac{p(z, \pi - |\Theta_b - \vartheta|)}{p(z, \pi)}[I_{\text{ss}}(z, \boldsymbol{\beta}, \boldsymbol{\vartheta}) \\
&+ I_{\text{mm}}(z, \boldsymbol{\beta}, \boldsymbol{\vartheta})],
\end{aligned}
\tag{41}
$$

where the coordinates are defined in the spherical frame of reference centered on the lidar position with the z axis chosen along the lidar axis; the angles from the lidar axis are assumed to be small; the sum is over all scattering orders N; Δ_1 is equal to the receiver field of view θ, and $\Delta_i = \infty$ for $i > 1$; $(z, \boldsymbol{\beta})$ are the coordinates of the illuminating radiance in plane z; $(z_i, \boldsymbol{\theta}_i)$ are the coordinates of the ith scattering position, with i taking all integer values between 1 and order N and $z_0 = \bar{z}$, $z_{N+1} = z$, $\boldsymbol{\theta}_0 = 0$, and $\boldsymbol{\theta}_{N+1} = \boldsymbol{\beta}$; Ω_i defines the solid angle through which the radiation scattered at $i + 1$ is collected by surface element $z_i^2 d^2\boldsymbol{\theta}_i$ at i; Θ_i is the scattering angle at i, and it is a function of $(z_i, \boldsymbol{\theta}_i)$, $(z_{i-1}, \boldsymbol{\theta}_{i-1})$, and $(z_{i+1}, \boldsymbol{\theta}_{i+1})$; Θ_b is the backscattering angle that depends on $(z_N, \boldsymbol{\theta}_N)$ and $(z, \boldsymbol{\beta})$; and $\boldsymbol{\vartheta}$ measures the angular direction of the illuminating radiance. Expression $\exp[-\tau(z)/2]$ gives the losses caused by absorption and wide-angle nondiffraction scatterings, and $\exp[-\tau(z)]$ is subtracted because the unscattered contributions have already been included in $P_{\text{un tot}}$.

It is obviously impractical to try to evaluate Eq. (41) exactly for N greater than 1. Instead, let us empirically represent the cumulative effects of the forward scatterings by a single function, $G(\theta, \beta)$, defined as follows:

$$
\begin{aligned}
&\sum_N\prod_{i=1}^N\int_0^{\Delta_i} d^2\boldsymbol{\theta}_i\int_{z_{i-1}}^{z} dz_i\Omega_i p(z_i, \Theta_i)\alpha_s(z_i) \\
&\quad\times p\,(z, \pi - |\boldsymbol{\Theta}_b - \boldsymbol{\vartheta}|) = G(\theta, \beta)\,\langle p(z, \pi - \vartheta)\rangle_{\theta_{pf}},
\end{aligned}
\tag{42}
$$

where $\langle p(z, \pi - \vartheta)\rangle_{\theta_{pf}}$ is the average of the backward phase function over a fluctuating scattering angle of standard deviation θ_{pf} about the value $\pi - \vartheta$; it is defined exactly as in Eq. (30).

The empirical function $G(\theta, \beta)$ is determined by analogy with the expression derived in the case of single scattering, i.e., for $P_{\text{ss un}} = P_{\text{un ss}}$. Thus, with reference to Eq. (38), we take

$$
\begin{aligned}
G(\theta, \beta) = \sqrt{\pi}\frac{C\theta}{\theta_{pf}}&[1 - \Phi(C\theta/\theta_{pf})] \\
&+ [1 - \exp(-C^2\theta^2/\theta_{pf}^2)] \qquad \text{for } \beta = 0.
\end{aligned}
\tag{43}
$$

Equation (43) is the angular profile of $P_{\text{ss un}} = P_{\text{un ss}}$, where width $1/A_1 y$ of the forward peak of the phase function has been replaced by width θ_{pf} of the convoluted phase function because of the multiple scatterings.

For $\theta \ll \beta$, the $\int^\theta d^2\boldsymbol{\theta}_1$ integration is over a domain that is small compared with β, and $G(\theta, \beta)$ is approximated by $\pi\theta^2$ times the profile of the backscattered radiance assumed of the same form as the profile of I_{ss}, i.e.,

$$
G(\theta, \beta) \approx \frac{\pi\theta^2}{2\sqrt{\pi}}\frac{C}{\theta_{pf}}\frac{1}{\beta}[1 - \Phi(C\beta/\theta_{pf})] \qquad \text{for } \theta \ll \beta.
\tag{44}
$$

For the same reason as in Eq. (43), θ_{pf} has been substituted for $1/A_1 y$.

Finally, the two limiting cases of Eqs. (43) and (44) are empirically linked together by the following single expression:

$$
\begin{aligned}
G(\theta, \beta) = \alpha_2\sqrt{\pi}&[1 - \Phi(\alpha_1)] + \exp[-(\beta/\theta)^2] \\
&\times [1 - \exp(-\alpha_1^2)],
\end{aligned}
\tag{45}
$$

where

$$
\alpha_1 = \frac{C}{\theta_{pf}}(\beta^2 + \theta^2)^{1/2},
\tag{46}
$$

$$
\alpha_2 = \frac{C}{\theta_{pf}}\frac{\theta^2}{\theta + 2\beta}.
\tag{47}
$$

The integrated effects of the inhomogeneous $p(z_i, \Theta_i)$'s of Eq. (42) are modeled in $G(\theta, \beta)$ by θ_{pf}, which

is itself the result of integrating the angular width of $p(z_i, \Theta_i)$ over the range from $\bar{z}$ to z.

With the help of Eqs. (42)–(47), Eq. (41) becomes

$$P_{ms\,ms}(z, \theta) = \frac{A}{z^2}\frac{ct}{2}\alpha_a(z)p(z, \pi)\exp[-\tau(z)] \times \{\exp[\tau(z)/2] - 1\} \times \int_0^\infty d^2\beta \int_0^\infty d^2\vartheta G(\theta, \beta)\frac{\langle p(z, \pi - \vartheta)\rangle_{\theta_{gf}}}{p(z, \pi)} \times [I_{ss}(z, \beta, \vartheta) + I_{mm}(z, \beta, \vartheta)]. \quad (48)$$

Substituting Eqs. (11) and (24) for I_{ss} and I_{mm} and using the approximations of Eqs. (33) and (34) and the definitions of Eqs. (29), (30), and (32), we have

$$P_{ms\,ms}(z, \theta) = P_{ss}(z)\{\exp[\tau(z)/2] - 1\}\int_0^\infty d^2\beta G(\theta, \beta) \times \left[\frac{1}{2\pi}\frac{A_2}{A_1}xy\frac{\sqrt{\pi}}{\beta}[1 - \Phi(A_1Cy\beta)] \times \frac{\langle p(z, \pi - 1/A_1yC)\rangle_{\theta_{gf}}}{p(z, \pi)} + \int_z^z dz'\frac{\alpha(z')}{2} \times (\exp\{[\tau(z) - \tau(z')]/2\} - 1) \times \frac{K}{\theta_{mm}^2}\left(\frac{\theta_{mm}}{\beta}\right)^{1/n}[1 - \Phi(\beta/\theta_{mm})] \times \frac{\langle p(z, \pi)\rangle_{\sqrt{2}\theta_{gf}}}{p(z, \pi)}\right]. \quad (49)$$

Defining

$$\delta_3(z, \theta) = \frac{\langle p(z, \pi - 1/A_1yC)\rangle_{\theta_{gf}}}{p(z, \pi)}, \quad (50)$$

$$\delta_4(z, \theta) = \frac{\langle p(z, \pi)\rangle_{\sqrt{2}\theta_{gf}}}{p(z, \pi)}, \quad (51)$$

we finally obtain

$$P_{ms\,ms}(z, \theta) = P_{ss}(z)\{\exp[\tau(z)/2] - 1\} \times \left[\frac{A_2}{A_1}xy\delta_3\int_0^\infty d\beta G(\theta, \beta)\sqrt{\pi} \times [1 - \Phi(A_1Cy\beta)] + \delta_4\int_z^z dz'\frac{\alpha(z')}{2} \times (\exp\{[\tau(z) - \tau(z')]/2\} - 1) \times 2\pi\int_0^\infty \beta d\beta G(\theta, \beta)\frac{K}{\theta_{mm}^2}\left(\frac{\theta_{mm}}{\beta}\right)^{1/n} \times [1 - \Phi(\beta/\theta_{mm})]\right]. \quad (52)$$

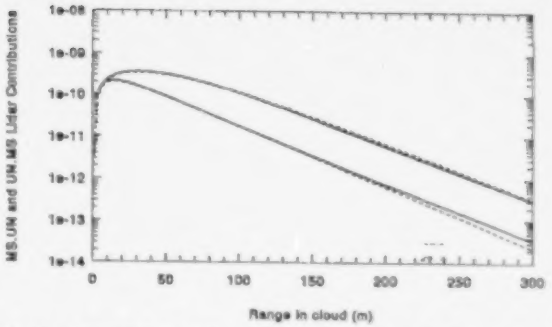

Fig. 2. Comparison of $P_{un\ ms}$ (dotted curve) and $P_{ms\ un}$ (solid curve), calculated at 0.5 mrad (lower curves) and 5 mrad (upper curves) for a homogeneous 300-m-thick C.1 cloud with an extinction coefficient equal to 17.25 km^{-1} located 1 km from the lidar.

There is a large degree of empiricism leading to Eq. (52) that makes detailed validation almost impossible. Comparisons with Monte Carlo calculations and experimental data are discussed in Section 3. Although these comparisons confirm the accuracy of the model for predicting the global effect of all contributions including $P_{ms\ ms}$, they cannot single out $P_{ms\ ms}$ from the other terms. However, we can use Eq. (40) to verify the consistency of the model. Equation (40) defines the equivalence between $P_{ms\ un}$ and $P_{un\ ms}$. An equation for $P_{ms\ un}$ can be obtained by substituting I_{un} for $I_{ss} + I_{mm}$ in Eq. (48). The result is

$$P_{ms\,un}(z, \theta) = P_{ss}(z)\{\exp[\tau(z)/2] - 1\} \times \frac{\langle p(z, \pi)\rangle_{\theta_{gf}}}{p(z, \pi)}G(\theta, 0), \quad (53)$$

for the case $\beta_0 \to 0$. From Eq. (38) in the same limit of $\beta_0 \to 0$ we have

$$P_{un\,ms}(z, \theta) = P_{ss}(z)\left[\frac{A_2}{A_1}\delta_1xy\sqrt{\pi}\left[\theta - \theta\Phi(A_1yC\theta) + \frac{1 - \exp(-A_1^2y^2C^2\theta^2)}{A_1yC\sqrt{\pi}}\right] + \delta_3\int_z^z dz'\frac{\alpha(z')}{2} \times (\exp\{[\tau(z) - \tau(z')]/2\} - 1) \times 2\pi\int_0^\theta \beta d\beta\frac{K}{\theta_{mm}^2}\left(\frac{\theta_{mm}}{\beta}\right)^{1/n} \times [1 - \Phi(\beta/\theta_{mm})]\right]. \quad (54)$$

These two expressions were derived by using related but quite different concepts. As a simple test, Eqs. (53) and (54) were calculated for the case of a 300-m-thick cloud of constant extinction coefficient set equal to 17.25 km^{-1}. The results are plotted in Fig. 2. Two sets of curves are shown that correspond to a field of view θ of 0.5 and 5 mrad, respectively. The

agreement between $P_{\mathrm{ms\ un}}$ and $P_{\mathrm{un\ ms}}$ is excellent almost everywhere. This by itself does not establish the accuracy of the model, but it certainly demonstrates the consistency of the hypotheses and approximations used and of the resulting empirical expressions for $P_{\mathrm{ms\ ms}}$.

The derivation is now complete. The resulting multiple-scattering lidar equation is obtained from Eqs. (25) and (39), i.e.,

$$P(z, \theta) = P_{\mathrm{un\ tot}}(z, \theta) + P_{\mathrm{ms\ un}}(z, \theta) + P_{\mathrm{ms\ ms}}(z, \theta). \tag{55}$$

Extracting $P_{\mathrm{ms\ un}} = P_{\mathrm{un\ ms}}$ from Eq. (38) and adding the result to the sum of Eqs. (38) and (52), we find

$$\begin{aligned} P(z, \theta) = P_{\mathrm{ss}}(z)\Bigg[& 1 - 2\frac{A_2}{A_1}\delta_1^2 xy\beta_0 \\ & \div \left[1 - \frac{2}{\pi}\tan^{-1}(A_1 yC\beta_0)\right] + 2\frac{A_2}{A_1}\delta_1 xy\sqrt{\pi} \\ & \times \left[\theta - \theta\Phi(A_1 yC\theta) + \frac{1 - \exp(-A_1^2 y^2 C^2\theta^2)}{A_1 yC\sqrt{\pi}}\right] \\ & + \frac{A_2}{A_1} xy\delta_3\{\exp[\tau(z)/2] - 1\} \\ & \times \int_0^\infty \mathrm{d}\beta G(\theta, \beta)\sqrt{\pi}[1 - \Phi(A_1 Cy\beta)] \\ & + \int_z^z \mathrm{d}z' \frac{\alpha(z')}{2}(\exp\{[\tau(z) - \tau(z')]/2\} - 1) \\ & \times 2\pi \int_0^\theta \beta\mathrm{d}\beta \frac{K}{\theta_{\mathrm{mm}}^2}\left(\frac{\theta_{\mathrm{mm}}}{\beta}\right)^{1/n}[1 - \Phi(\beta/\theta_{\mathrm{mm}})] \\ & \times (2\delta_2 + \delta_4\{\exp[\tau(z)/2] - 1\}G(\theta, \beta))\Bigg]. \end{aligned} \tag{56}$$

Here $P(z, \theta)$ is the total lidar power received from range z and within a field of view θ; $P_{\mathrm{ss}}(z)$, $\theta_{\mathrm{mm}}(z, z')$, $K(z, z')$, $\theta_{\mathrm{pr}}(z)$, C, n, $G(\theta, \beta)$, δ_1, δ_2, δ_3, and δ_4 are given by Eqs. (32), (16), (20), (23), (12), (18), (45), (35), (36), (50), and (51), respectively.

Equation (56) constitutes the main result of this paper. It gives the multiple-scattering lidar equation in the form of the conventional single-scattering expression $P_{\mathrm{ss}}(z)$, multiplied by a sum of terms that depend on medium parameters $x = z\alpha(z)$ and $y = \pi d(z)/\lambda$, the optical depth $\tau(z)$ measured along the lidar axis, and the receiver field of view θ. It is valid for phase functions characterized by a narrow forward peak, i.e., $1/A_1 y \ll 1$, and for fields of view θ greater than the laser pulse divergence β_0, i.e., $\theta^2 \gg \beta_0^2$, but smaller than the width of the phase function peak, i.e., $\theta < 1/CA_1 y$. The geometrical-optics wide-angle scatterings were treated as losses.

The proposed multiple-scattering lidar equation, Eq. (56), permits the separation of the various contributions to the lidar returns into the following individual terms: (a) unscattered backward ⊙ unscattered forward, where ⊙ stands for convolution, i.e.,

$$P_{\mathrm{un\ un}} = P_{\mathrm{ss}}(z);$$

(b) unscattered backward ⊙ singly scattered forward and *vice versa*, i.e.,

$$\begin{aligned} P_{\mathrm{un\ ss}} + P_{\mathrm{ss\ un}} = P_{\mathrm{ss}}(z)\Bigg\{ & -2\frac{A_2}{A_1}\delta_1^2 xy\beta_0 \\ & \div \left[1 - \frac{2}{\pi}\tan^{-1}(A_1 yC\beta_0)\right] \\ & + 2\frac{A_2}{A_1}\delta_1 xy\sqrt{\pi}\Bigg[\theta - \theta\Phi(A_1 yC\theta) \\ & + \frac{1 - \exp(-A_1^2 y^2 C^2\theta^2)}{A_1 yC\sqrt{\pi}}\Bigg]\Bigg\}; \end{aligned}$$

(c) unscattered backward ⊙ scattered more than once forward and *vice versa*, i.e.,

$$\begin{aligned} P_{\mathrm{un\ mm}} + P_{\mathrm{mm\ un}} = P_{\mathrm{ss}}(z)\Bigg[& 2\delta_2 \int_z^z \mathrm{d}z' \frac{\alpha(z')}{2} \\ & \times (\exp\{[\tau(z) - \tau(z')]/2\} - 1) \\ & \times 2\pi \int_0^\theta \beta\mathrm{d}\beta \frac{K}{\theta_{\mathrm{mm}}^2}\left(\frac{\theta_{\mathrm{mm}}}{\beta}\right)^{1/n} \\ & \times [1 - \Phi(\beta/\theta_{\mathrm{mm}})]\Bigg]; \end{aligned}$$

(d) multiply scattered backward ⊙ singly scattered forward, i.e.,

$$\begin{aligned} P_{\mathrm{ms\ ss}} = P_{\mathrm{ss}}(z)\Bigg(& \frac{A_2}{A_1} xy\delta_3\{\exp[\tau(z)/2] - 1\} \\ & \times \int_0^\infty \mathrm{d}\beta G(\theta, \beta)\sqrt{\pi}[1 - \Phi(A_1 Cy\beta)]\Bigg); \end{aligned}$$

and (e) multiply scattered backward ⊙ scattered more than once forward, i.e.,

$$\begin{aligned} P_{\mathrm{ms\ mm}} = P_{\mathrm{ss}}(z)\Bigg[& \delta_4\{\exp[\tau(z)/2] - 1\} \\ & \times \int_z^z \mathrm{d}z' \frac{\alpha(z')}{2}(\exp\{[\tau(z) - \tau(z')]/2\} - 1) \\ & \times 2\pi \int_0^\theta \beta\mathrm{d}\beta\, G(\theta, \beta) \frac{K}{\theta_{\mathrm{mm}}^2}\left(\frac{\theta_{\mathrm{mm}}}{\beta}\right)^{1/n} \\ & \times [1 - \Phi(\beta/\theta_{\mathrm{mm}})]\Bigg]. \end{aligned}$$

P500609.PDF [Page: 13 of 22]

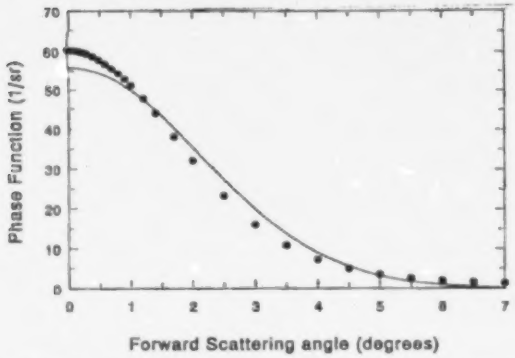

Fig. 3. Forward peak of the C.1 cloud, 1.06-μm phase function. Circles, Mie calculations; solid curve, Gaussian fit given by Eq. (6) with $A_1 = 0.544$, $A_2 = 0.139$, and $d = 12$ μm.

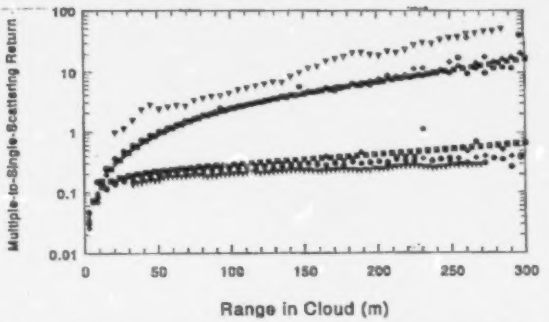

Fig. 4. Comparisons of predictions derived from Eq. (56) with Monte Carlo calculations of Ref. 9 for lidar returns at 1.06 μm from a uniform 17.25-km^{-1} C.1 cloud at a distance of 1 km. Circles, Florence group; triangles, Israel group; diamonds, Munich group; and squares, Eq. (56). The receiver fields of view are 0.5 and 5 mrad for the lower and upper curves, respectively.

3. Direct Problem

Equation (56) is used first to calculate the lidar return for a simple numerical experiment. The experiment is the same as that defined for the intercomparison study of Ref. 9. The lidar source is a pulsed Nd:YAG 1.064-μm laser of 0.1-mrad divergence, vanishing beam waist, and 40-ns pulse duration. The cloud is at a distance of 1000 m and consists of a Deirmendjian[13] C.1 water droplet concentration given by

$$\frac{dN}{dr} = N_0 r^6 \exp(-1.5r), \tag{57}$$

where N is the particle concentration, r is the droplet radius, and N_0 is a constant. The cloud scattering properties were calculated with Mie theory. The particle refractive index was taken to be $m = 1.325 + 0i$, i.e., $\omega = 1$, and the constant N_0 of Eq. (57) was adjusted to give an extinction coefficient of 17.25 km^{-1}. The size distribution was cut off at 0.01 μm at the low end and 20 μm at the high end of the distribution. The receiver is coaxial with the laser, and the calculations were performed for two fields of view, i.e., 0.5 and 5 mrad half-angles.

Constants A_1 and A_2 of Eq. (6) were determined by fitting the Gaussian function to the forward peak of the phase function calculated with Mie theory for the angular interval between zero and the point where the function drops to 5% of its peak value. The effective particle diameter that enters Eq. (6) was set equal to 12 μm, i.e., the value obtained from Eq. (57) by applying the definition of $d = 2\langle r^3\rangle/\langle r^2\rangle$, and $\omega = 1$. The resulting numerical constants are $A_1 = 0.544$ and $A_2 = 0.139$. Figure 3 illustrates the quality of the fit. The fraction of scattered radiation contained in the fitted peak function, i.e.,

$$2\pi \int_0^{\infty} \frac{A_2}{\omega\pi} y^2 \exp(-A_1^2 y^2 \theta^2)\theta d\theta = \frac{A_2}{\omega A_1^2} = 0.47, \tag{58}$$

agrees well with the theoretical value of 1/2 for diffraction used throughout this paper.

Figure 4 compares the predictions derived from Eq. (56) with Monte Carlo calculations performed by the Florence group,[14] the Munich group,[15] and the Israel group.[16] and collected together in the intercomparison study discussed in Ref. 9. The agreement is good for both the range and field-of-view dependences, except that the present model predicts a slightly greater multiple-scattering effect at the smallest field of view. Figure 3 shows that the Gaussian fit to the Mie phase function is flatter at $\theta = 0$. Hence, the integral over the solid angle, i.e., the angular probability distribution of the scatterings, has a greater slope at $\theta = 0$, which could explain the differences observed at 0.5 mrad. The Monte Carlo solutions were calculated with the full Mie function.

Monte Carlo methods are considered to be good mathematical representations of multiple-scattering processes. However, they remain models and cannot be universally substituted for experimental data. There are numerous lidar measurements reported in the literature, but truly independent validation data are rare because the atmosphere is highly variable and difficult to characterize on the temporal and spatial domains achievable with lidars. A few laboratory simulations have been performed to fill this need. In particular, a group at the University of Florence[17] has recently achieved range-resolved multiple-scattering lidar measurements from a well-characterized test cell under controlled laboratory conditions. The high spatial resolution was obtained from a short 4-ps dye laser pulse at 766.5 nm. The scattering medium consisted of a water suspension of polystyrene spherical particles of known concentration and size distribution. Homogeneous conditions were ensured by stirring. The cell length and diameter were, respectively, 100 and 80 mm. The returns from the cell were measured with a streak camera having a response time of 25 ps, cor-

P500609.PDF [Page: 14 of 22]

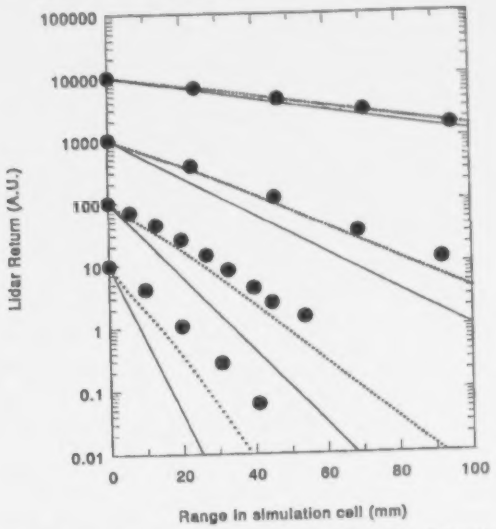

Fig. 5. Comparisons of predictions derived from Eq. (56) with the laboratory simulation data of Ref. 17 for the scattering coefficients, from top to bottom, of 0.006, 0.030, 0.060, and 0.132 mm^{-1}. Circles, measurements; dotted curves, Eq. (56); and solid curves, single-scattering solutions.

responding to a spatial resolution of 2.8 mm. The camera was placed 250 mm in front of the cell and aligned coaxially with the laser beam. The camera aperture and field of view were, respectively, 0.2 mm and 6.1 mrad half-angle.

Lidar echos were reported for four extinction coefficients and two size distributions with average particle diameters of 0.09 and 5.4 μm. The 0.09-μm results are not considered here, because for these very small particles there is no strong forward diffraction peak required for the validity of Eq. (56), and there is hardly any measurable multiple scattering as evident from the results of Ref. 17. The returns recorded from the 5.4-μm particle suspension are compared with the predictions of Eq. (56) in Fig. 5 for the four scattering coefficients of 0.006, 0.03, 0.063, and 0.132 mm^{-1}. The scattering phase function was calculated with Mie theory for the particle-size distribution and optical properties given in Ref. 17. The particles are nonabsorbing, i.e., $\omega = 1$, but the water medium has an absorption coefficient of 0.0025 mm^{-1}. The same constants $A_1 = 0.544$ and $A_2 = 0.139$ as in the previous example were used, and fitting Eq. (6) to the phase-function peak yielded an effective particle diameter of $d = 5.7$ μm, in good agreement with the value of $d = 2\langle r^3\rangle/\langle r^2\rangle = 5.6$ μm derived from the given size distribution. The experimental data were reported in arbitrary units and have been adjusted for a perfect match at zero range and to separate the results at the different extinction values. Also plotted as continuous lines are the corresponding single-scattering solutions that illustrate the magnitude of the multiple-scattering effects.

The comparisons of Fig. 5 show that the multiple-scattering contributions grow with the optical depth and that there is good agreement between the measurements and the predictions of Eq. (56), except for the denser media where the predictions are low. The agreement is still acceptable at 0.063 mm^{-1} but is rather poor at 0.132 mm^{-1}. Zaccanti *et al.*[17] estimate their experimental errors on the slope of the measured data to be 10%. The observed difference in Fig. 5 between the slopes of the measured and predicted returns at 0.132 mm^{-1} is almost 30%. Therefore, the experimental errors alone cannot explain the discrepancy observed in that case. The model underestimates the multiple-scattering contributions because it neglects the wide-angle scatterings. The effect is in the right direction, but it is not certain whether it is sufficient to reconcile the predictions with the measurements.

In conclusion, the combined results of Figs. 4 and 5 show that the model performs well in most situations studied. There is only one case of very dense media on a reduced laboratory scale in which the differences are large and yet unexplained.

4. Inverse Problem

The main purpose of the proposed model was to develop a formulation of the multiple-scattering lidar equation that was simple enough to allow inversion. The result is Eq. (56). The objective of the inverse problem is to solve for $x(z)$ and $y(z)$, i.e., the extinction coefficient $\alpha(z)$ and the particle effective diameter $d(z)$ by fitting Eq. (56) to lidar returns measured at three or more fields of view simultaneously.

Equation (56) is still rather complicated. The dependence on x and y is both explicit and implicit through optical depth τ and functions θ_{mm}^2, θ_{pf}^2, K, and G. We treat the implicit dependence by an iterative method using the preceding approximation to evaluate the terms involving τ, θ_{mm}^2, θ_{pf}^2, K, and G. These terms involve integrals over range z; they contribute little at short ranges, and at long ranges where they become significant, they are less and less dependent on the local $\alpha(z)$ and $d(z)$. In other words, the iteration is generally stable and converges rapidly. At each iteration step, the new approximations for x and y are calculated by least-squares fitting Eq. (56), with the implicit terms fixed by substituting the values of x and y from the preceding step to the measured returns at the various fields of view. One can eliminate the single-scattering expression P_{ss} by ratioing all the returns to the smallest field-of-view return. The solution starts at the point where sufficient multiple scattering is measured. This can be easily determined by thresholding the ratio of the returns at two adjacent fields of view. Thus far, it has been found that the method works well to optical depths of ~4. At greater depths, the explicit terms in Eq. (56) become small compared with the implicit terms, which makes the solutions increasingly sensitive to errors.

As a way to illustrate the method, simulated multiply scattered lidar returns were calculated with Eq. (56). A 300-m-thick water cloud ($\omega = 1$) was as-

P500609.PDF [Page: 15 of 22]

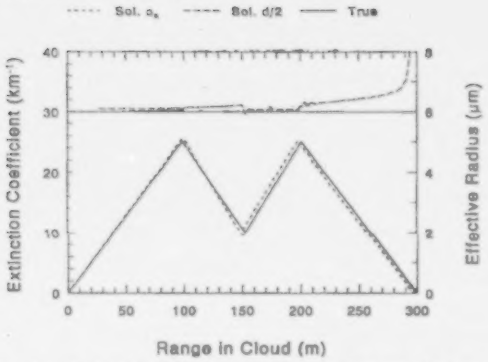

Fig. 6. Inversion solutions for extinction coefficient α (left vertical scale) and effective particle radius $d/2$ (right vertical scale) for a C.1 cloud at a distance of 1 km. Lidar signals at fields of view of 0.5, 1.5, 2.5, and 5 mrad were calculated with Eq. (56) for the true particle size and extinction coefficient profiles plotted as continuous curves. Solutions were obtained for backward phase-function ratios $\delta_1 = \delta_2 = \delta_3 = \delta_4$ set equal to 0.7, which is the value used for the direct calculation.

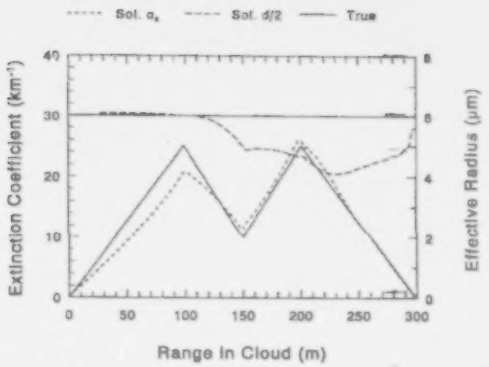

Fig. 7. Same as Fig. 6, except for $\delta_1 = \delta_2 = \delta_3 = \delta_4 = 1$.

sumed with a double-peak sawtooth profile for a total optical depth of 4.25. The same C.1 phase function as in Fig. 3 was used for the computations. The cloud was positioned at a distance of 1 km from the lidar and the returns were calculated at four fields of view, namely, 0.5-, 1.5-, 2.5-, and 5-mrad half-angles.

One difficulty of the inversion is that backscatter ratios δ_1 through δ_4 are not known *a priori*. The results obtained with $\delta_1 \simeq \delta_2 \simeq \delta_3 \simeq \delta_4$ set equal to the value of 0.7 calculated from the C.1 cloud phase function and used for the direct problem are plotted in Fig. 6. The inversion gives back the input data very well. The profile of the extinction coefficient is reproduced to within ~2%, and the effective radius solution approximates the true value of 6 μm with a precision of ~10%, except at the top of the cloud, where the lidar signals drop to zero. The solution begins at 25 m, which is the point where the multiple-scattering strength satisfies our preset threshold. For α the solution is extended back to zero by means of the single-scattering solution, with the boundary value provided by the first multiple-scattering solution point at 25 m.

The good solutions illustrated in Fig. 6 were of course expected because the same model was used for the direct and inverse problems. The purpose was to demonstrate that the iterative solution algorithm works and is accurate for returns determined at a few discrete fields of view, as would be the case in practical applications.

The inversion solutions obtained with $\delta_1 = \delta_2 = \delta_3 = \delta_4 = 1$, the most likely first approximation for unknown δ's, are plotted in Fig. 7. The solution for the extinction coefficient is not drastically affected, but the precision on the effective radius decreases with penetration depth. The important point is that the inversion can handle signal and model errors, here equal to ~30% in the strength of the multiple-scattering contributions, without catastrophic consequences. Of course, the resulting solution profiles are affected but the errors are more or less of the same order of magnitude as the errors on the δ's.

The dependence of the multiple-scattering contributions on the backscatter properties of the aerosol medium, even after ratioing with the smallest field-of-view return, remains a difficulty for the inversion problem. Ratios δ_1 through δ_4 are not known, and some form of algorithm will be needed to estimate them. However, compared with the backscatter-to-extinction ratio of the single scattering equation, the δ's have a much smaller range of uncertainty, especially for natural aerosols, which generally have broad size distributions. For example, we find that the δ's vary from a value near unity to a value of ~0.7 for conditions ranging from haze to clouds.

Figure 7 shows that the solution for the effective particle size is initially unaffected by uncertainties on the δ's. This suggests that an algorithm based on some general knowledge of the medium under study, e.g., clouds, could be worked out to estimate the δ's from the solution for d at the previous step. The precision of such relations need not be superior to ~10% to improve significantly the accuracy of the solutions.

In Ref. 10, an early version of the present model was used to invert experimental lidar data measured at three fields of view. The results were compared with independent *in situ* extinction and transmittance measurements obtained in two separate field experiments. That research was done independently of the simulation studies of this paper. In particular, the δ's were set equal to unity, and constants A_1 and A_2 were chosen to optimize the fit between solutions and measurements. Good agreement was found in all cases with $A_1 = 0.4$ and $A_2 = 0.1$. The experiments of Ref. 10 were carried out separately from the simulations of this paper, and the resulting 30% differences in A_1 and A_2 are not great at this stage in the development of the inversion method, considering all possible error sources, e.g., lidar measurements, *in situ* sensor measurements, the accuracy of the model, and the 30% uncertainties

P500609.PDF [Page: 16 of 22]

on the δ's. More simulations and investigations with other lidars are necessary, but the outlook is promising. The advantages of being able to derive remotely and from a single instrument the range-resolved extinction coefficient and effective particle size of dense particulate media are certainly worth pursuing.

5. Conclusion

A multiple-scattering lidar equation was derived. The formulation explicitly shows the dependence on extinction coefficient $\alpha(z)$ and effective particle diameter $d(z)$. As a result, lidar signals containing multiple-scattering contributions can be inverted to give $\alpha(z)$ and $d(z)$ through a straightforward numerical algorithm. The situation modeled by the proposed multiple-scattering lidar equation is that of multiple forward scatterings in both the direct and return paths, and a single backscattering at an angle close to π. The model postulates that the scatterings contributing to the lidar returns are the diffraction scatterings; the residual wide-angle geometrical-optics scatterings are taken into account as a loss mechanism only. In addition, the effective size parameter is assumed to be large enough for the diffraction scatterings to make up one half of the extinction coefficient. The resulting domain of validity is thus restricted to fields of view θ such that $z\theta < (z - \bar{z})\theta_d$, where $\bar{z}$ is the range to the cloud of interest and $\theta_d = 1/A_1 y$ is the width of the diffraction peak of the scattering phase function, and to optical depths less than approximately 5. Many lidar applications meet these requirements. Corrections could be worked out to take into account the geometrical-optics scatterings in order to extend the domain of validity to greater fields of view. However, for inversion purposes, it is preferable to keep the fields of view small to ensure that the dependence on the particle size is as simple as possible.

Lidar signals calculated with the multiple-scattering equation of this paper are in good agreement with the Monte Carlo calculations of Ref. 9. The agreement is also quite satisfactory with the laboratory measurements of Zaccanti *et al.*,[17] except for one case of very dense, i.e., extinction coefficient greater than 0.1 mm^{-1}, particle concentration. Numerical simulations show that the inversion is possible and that it can withstand model and signal errors of ~30% without serious consequences, i.e., the resulting solution errors are of the same order of magnitude. No boundary value is needed. However, the relative value of the phase function near the backscatter direction must be estimated in the form of the average parameters δ's defined in the paper, and the precision on the calculated multiple-scattering contributions is directly proportional to the precision on the δ's. It is emphasized that it is only the average phase function relative to the value at π that has to be specified, and only over an angular range of the order of the width of the forward peak. For given classes of aerosols such as fog and clouds, it may be possible to develop iterative algorithms to estimate the δ's in terms of the solution for the effective particle size. Depolarization measurements might also prove to be a valuable source of information on the δ's.

Appendix A: List of Symbols

The following is an abridged list of the main symbols and definitions used in this paper.

C	geometric factor, $C = z/(z - \bar{z})$;
d	effective particle diameter defined as the ratio of the third-order to the second-order moment of the size probability density function;
p	scattering phase function;
I_{un}	unscattered radiance;
I_{ss}	singly scattered radiance;
I_{mm}	multiply (≥2) scattered radiance;
$P(z, \theta)$	lidar signal from range z within field of view θ, equal to $P_{un\,un} + P_{ss\,un} + P_{mm\,un} + P_{un\,ss} + P_{ms\,ss} + P_{un\,mm} + P_{ms\,mm}$;
$P_{un\,un}$	contribution to lidar return, unscattered-backward ⊙ unscattered-forward;
$P_{un\,ss}$	contribution to lidar return, unscattered backward ⊙ singly scattered forward;
$P_{un\,mm}$	contribution to lidar return, unscattered backward ⊙ scattered more than once forward;
$P_{ss\,un}$	contribution to lidar return, singly scattered backward ⊙ unscattered forward;
$P_{mm\,un}$	contribution to lidar return, scattered more than once backward ⊙ unscattered forward;
$P_{ms\,ss}$	contribution to lidar return, multiply (≥1) scattered backward ⊙ singly scattered forward;
$P_{ms\,mm}$	contribution to lidar return, multiply (≥1) scattered backward ⊙ scattered more than once forward;
$x = z\alpha_s$	is the nondimensional scattering coefficient;
$y = \pi d/\lambda$	is the size parameter;
z	range;
$\bar{z}$	range to cloud boundary;
$(z, \beta) = (z, \beta, \phi)$	is the coordinates in the backscattering plane;
$(z_i, \theta_i) = (Z_i, \theta_i, \phi_i)$	is the coordinates of the ith scattering center;
α	extinction coefficient;
α_s	scattering coefficient;
β_0	lidar beam divergence;

P500609.PDF [Page: 17 of 22]

δ's normalized average backward phase function over the angular domain of the backscatterings that contribute to the received lidar signal; there is one δ for each of the multiple-scattering terms (four in all), but they do not differ much from one another

θ lidar receiver field of view;

$\vartheta = (\vartheta, \varphi)$ is the angular coordinates of radiance;

$\tau = \int_{\tilde{z}}^{z} \alpha dz$ is the optical depth;

$\omega = \alpha_s/\alpha$ is the single-scattering albedo;

$\odot$ denotes convolution.

Appendix B: Finite Beam Effect

Equation (11) for the single-scattering contribution to the illumination was derived under the assumption that the laser beam divergence, β_0, is infinitesimally small. This has led to a $1/\beta$ dependence of I_{ss} as $\beta \to 0$. In reality, β_0 is finite and the behavior of I_{ss} near $\beta = 0$ must be modified.

Substituting Eq. (6) for p and Eq. (4) for θ' in Eq. (5), using the definition $\alpha = \alpha_s/\omega$, performing the integrations over ϕ' and β', and letting $\beta \to 0$, we have

$$\lim_{\beta \ll \beta_0} I_{ss}(z, \boldsymbol{\beta}, \boldsymbol{\vartheta}) = \frac{A_2}{\pi} P_0 \exp[-\tau(z)] \times \int_{\tilde{z}}^{z} dz' \frac{\alpha(z')z^2}{(z-z')^2} y^2(z') \times \frac{\delta(\vartheta)}{[1 + A_1^2 y^2(z') z^2 \beta_0^2/(z-z')^2]}. \quad \text{(B1)}$$

The integrand of Eq. (B1) peaks at $z' = z$. Setting $\alpha(z') \simeq \alpha(z)$ and $y(z') \simeq y(z)$, we can perform the z' integration to yield

$$\lim_{\beta \ll \beta_0} I_{ss}(z, \boldsymbol{\beta}, \boldsymbol{\vartheta}) = \frac{A_2}{\pi A_1} P_0 \exp[-\tau(z)] \frac{xy}{\beta_0} \times \left[\frac{\pi}{2} - \tan^{-1}(A_1 y C \beta_0)\right] \delta(\boldsymbol{\vartheta}), \quad \text{(B2)}$$

where x and y are defined in Eqs. (33) and (34). With reference to Eq. (26), the contribution to the lidar returns from this term, assuming no scattering in the backward direction, is given by

$$\lim_{\theta \ll \beta_0} P_{\text{un ss}}(z, \theta) = \frac{ct}{2} \frac{A}{z^2} \exp[-\tau(z)] \alpha_s(z) p(z, \pi) 2\pi \times \int_0^{\theta} \beta d\beta \int_0^{2\pi} d\phi \int_0^{\infty} \vartheta d\vartheta \times \lim_{\beta \ll \beta_0} I_{ss}(z, \boldsymbol{\beta}, \boldsymbol{\vartheta}) \frac{p(z, \pi - |\boldsymbol{\beta} - \boldsymbol{\vartheta}|)}{p(z, \pi)}, \quad \text{(B3)}$$

or after using Eq. (B2) and integrating

$$\lim_{\theta \ll \beta_0 \ll 1} P_{\text{un ss}}(z, \theta) = P_{ss}(z) \frac{A_2}{A_1} \frac{xy}{\beta_0} \times \left[\frac{\pi}{2} - \tan^{-1}(A_1 y C \beta_0)\right] \theta^2. \quad \text{(B4)}$$

It was assumed in deriving Eq. (B4) that

$$\frac{p(z, \pi - \beta)}{p(z, \pi)} \simeq 1 \quad \text{(B5)}$$

for $\beta \leq \theta \ll \beta_0 \ll 1$.

Equation (B4) must be compared with the limit of the expression obtained in the main article for $P_{\text{un ss}}$ under the condition $\beta_0 \ll \theta \ll 1/A_1 y$, i.e., from Eq. (37)

$$\lim_{\beta_0 \ll \theta \ll 1/A_1 Cy} P_{\text{un ss}}(z, \theta) = P_{ss}(z) \frac{A_2}{A_1} \delta_1 xy \sqrt{\pi} \theta. \quad \text{(B6)}$$

To determine the effect of the finite beam divergence on the measured returns, we must match the θ^2 asymptote of Eq. (B4) to the θ asymptote of Eq. (B6). To do this, we propose a function of the form

$$\mathcal{F} = \mathcal{A}[\exp(-\mathcal{B}\theta) - 1] + \mathcal{A}\mathcal{B}\theta, \quad \text{(B7)}$$

which has the required quadratic and linear asymptotes in the limits $\theta \to 0$ and $\theta \to \infty$, respectively. With this notation, the downward shift in $P_{\text{un ss}}(z, \theta)$ caused by the finite size β_0 of the laser pulse is equal to $-\mathcal{A}$. One can easily derive a solution for $\mathcal{A}$ by equating the limit of $\mathcal{F}$ for $\theta \to \infty$ to Eq. (B6) and the limit of $\mathcal{F}$ for $\theta \to 0$ to Eq. (B4). The result is

$$\mathcal{A} = P_{ss}(z) \frac{A_2}{A_1} \delta_1^2 xy \beta_0 \left[1 - \frac{2}{\pi} \tan^{-1}(A_1 y C \beta_0)\right]^{-1}. \quad \text{(B8)}$$

One can subtract this expression for $\mathcal{A}$ from Eq. (37) to correct for the finite beam effect, and the result is Eq. (38).

Appendix C: Equivalence Between Scattered Forward, Unscattered Backward and Unscattered Forward, Scattered Backward

The single-scattering part of the left-hand side of Eq. (40), i.e., $P_{\text{ss un}}$, can be derived analytically in exact form. Indeed, lidar contribution $P_{\text{ss un}}(z, \theta)$ from the radiation unscattered in the forward direction, backscattered through an angle $\pi - \theta'$ at z, scattered once at z' between z and zero on the return leg, and collected within a field-of-view angle θ at the receiver is

given by

$$P_{ss\,un}(z,\theta) = \int_0^{2\pi}\int_0^{\theta}\int_z^{z} \{P_0 \exp[-\tau(z)]\} \times \left\{\exp[-\tau(z)+\tau(z')]\alpha_s(z)p(z,\pi-\theta')\frac{ct}{2}\right\} \times \left[\frac{z'^2\cos(\beta+\theta')\mathrm{d}\phi\beta\mathrm{d}\beta}{(z-z')^2/\cos^2\theta'}\right] \times \left\{\alpha_s(z')p(z',\beta+\theta')\frac{\mathrm{d}z'}{\cos\theta'} \times \exp[-\tau(z')]\frac{A}{z'^2}\right\}. \quad \text{(C1)}$$

For simplicity, Eq. (C1) was written for a lidar pulse of vanishing divergence. The first group of terms in braces is the incident unscattered power at z, the second group in braces gives the fraction backscattered through angle $\pi - \theta'$ and reaching z', the first group in brackets is the element of solid angle subtended by surface element $z'^2\beta\mathrm{d}\beta\mathrm{d}\phi$ from the backscattering position, and the third group in braces gives the amount rescattered at z' toward the receiver and actually collected by a receiver of aperture area A. Under the same condition of small angles as assumed throughout, we have

$$\theta' \simeq \frac{z'}{z-z'}\beta, \quad \text{(C2)}$$

$$\cos\theta' \simeq 1, \quad \text{(C3)}$$

$$\cos(\beta+\theta') \simeq 1. \quad \text{(C4)}$$

Using these simplifications and rearranging Eq. (C1), we find

$$P_{ss\,un}(z,\theta) = P_0\exp[-2\tau(z)]\frac{ct}{2}\frac{A}{z^2}\alpha_s(z)p(z,\pi)2\pi \times \int_0^{\theta}\beta\mathrm{d}\beta\int_z^{z}\mathrm{d}z'\frac{z^2}{(z-z')^2}\alpha_s(z') \times p\left(z',\frac{z}{z-z'}\beta\right)\frac{p[z,\pi-(z'/z-z')\beta]}{p(z,\pi)}. \quad \text{(C5)}$$

Substituting Eq. (5) for I_{ss} with $\beta_0 \to 0$ in Eq. (26), for the reverse $P_{un\,ss}$ we find

$$P_{un\,ss}(z,\theta) = P_0\exp[-2\tau(z)]\frac{ct}{2}\frac{A}{z^2}\alpha_s(z) \times p(z,\pi)2\pi\int_0^{\theta}\beta\mathrm{d}\beta \times \int_0^{2\pi}\mathrm{d}\phi\int_0^{\infty}\vartheta\mathrm{d}\vartheta\int_z^{z}\mathrm{d}z'\frac{z^2}{(z-z')^2}\alpha_s(z') \times p(z',\theta')\frac{p(z,\pi-|\beta-\vartheta|)}{p(z,\pi)}\delta(\vartheta-\theta'). \quad \text{(C6)}$$

Using approximation (C2) for θ' and performing the integration over ϑ, we obtain

$$P_{un\,ss}(z,\theta) = P_0\exp[-2\tau(z)]\frac{ct}{2}\frac{A}{z^2}\alpha_s(z)p(z,\pi)2\pi \times \int_0^{\theta}\beta\mathrm{d}\beta\times\int_z^{z}\mathrm{d}z'\frac{z^2}{(z-z')^2}\alpha_s(z') \times p\left(z',\frac{z}{z-z'}\beta\right)\frac{p[z,\pi-(z'/z-z')\beta]}{p(z,\pi)}. \quad \text{(C7)}$$

Equations (C5) and (C7) are identical, which demonstrates that

$$P_{ss\,un} = P_{un\,ss} \quad \text{(C8)}$$

for a medium of arbitrary phase function and scattering coefficient.

I am indebted to P. Bruscaglioni, A. Cohen, and A. V. Starkov for providing the Monte Carlo simulation results of Fig. 4, and to G. Zaccanti and P. Bruscaglioni for the experimental data of Fig. 5. I also thank Gilles Roy and François Nicolas for numerous helpful discussions.

References

1. R. J. Allen and C. M. R. Platt, "Lidar for multiple backscattering and depolarization observations," Appl. Opt. **16**, 3193–3199 (1977).
2. S. R. Pal and A. I. Carswell, "Polarization properties of lidar scattering from clouds at 347 nm and 694 nm," Appl. Opt. **17**, 2321–2328 (1978).
3. K. Sassen and R. L. Petrilla, "Lidar depolarization from multiple scattering in marine stratus clouds," Appl. Opt. **25**, 1450–1459 (1986).
4. L. R. Bissonnette and D. L. Hutt, "Multiple scattering lidar," Appl. Opt. **29**, 5045–5046 (1990).
5. C. Werner, J. Streicher, H. Herrmann, and H.-G. Dahn, "Multiple-scattering lidar experiments," Opt. Eng. **31**, 1731–1745 (1992).
6. D. L. Hutt, L. R. Bissonnette, and L. Durand, "Multiple field of view lidar returns from atmospheric aerosols," Appl. Opt. **33**, 2338–2348 (1994).
7. E. W. Eloranta, "Calculation of doubly scattered lidar returns," Ph.D. dissertation (University of Wisconsin, Madison, Wisc., 1972).
8. C. M. R. Platt, "Lidar and radiometer observations of cirrus clouds," J. Atmos. Sci. **30**, 1191–1204 (1973).
9. L. R. Bissonnette, P. Bruscaglioni, A. Ismaelli, G. Zaccanti, A. Cohen, Y. Benayahu, M. Kleiman, S. Egert, C. Flesia, P. Schwendimann, A. V. Starkov, M. Noormohammadian, U. G. Oppel, D. M. Winker, E. P. Zege, I. L. Katsev, and I. N. Polonski, "Lidar multiple scattering from clouds," Appl. Phys. B **60**, 355–362 (1995).

P500609.PDF [Page: 19 of 22]

10. L. R. Bissonnette and D. L. Hutt, "Multiply scattered aerosol *lidar returns: inversion method and comparison with in situ* measurements," Appl. Opt. **34,** 6959–6975 (1995).
11. L. R. Bissonnette, "Multiscattering model for propagation of narrow light beams in aerosol media," Appl. Opt. **27,** 2478–2484 (1988).
12. L. R. Bissonnette, "Multiple scattering of narrow light beams in aerosols," Appl. Phys. B **60,** 315–323 (1995).
13. D. Deirmendjian, "Far-infrared and submillimeter wave attenuation by clouds and rain," J. Appl. Meteorol. **14,** 1584–1593 (1975).
14. P. Bruscaglioni, A. Ismaelli, and G. Zaccanti, "Monte Carlo calculations of lidar returns: procedure and results of Florence group," Appl. Phys. B **60,** 325–329 (1995).
15. A. V. Starkov, M. Noormohammadian, and U. G. Oppel, "A stochastic model and a variance reduction Monte Carlo method for calculation of light transport," Appl. Phys. B **60,** 335–340 (1995).
16. A. Cohen, M. Kleiman, and J. Cooney, "Lidar measurements of rotational Raman and double scattering," Appl. Opt. **16,** 1905–1910 (1978).
17. G. Zaccanti, P. Bruscaglioni, M. Gurioli, and P. Sansoni, "Laboratory simulations of lidar returns from clouds: experimental and numerical results," Appl. Opt. **32,** 1590–1597 (1993).

Defence Research and Development Canada | Recherche et développement pour la défense Canada | Canada

Français Contact Us Help Search Canada Site
Home Defence R&D Canada Defence Site

Browse Indexes

Titles
Authors
Descriptors
Corporate Authors
Corporate Acronyms
Report Numbers
Search Database
Summary

It is recommended you search "Authors" and "Corporate Authors" on their respective "Browse" pages.

Click here if you are having problems displaying text (ie. text is too big, or too small) or page appears to be jumbled.

Prior Top **Document:** 3 of 7 Bottom Next
Click here to Order
Click here to Download

TITLE:(U) MULTIPLE-SCATTERING LIDAR EQUATION
PERSONAL AUTHOR: Bissonnette, L.R.
CORPORATE AUTHOR: Defence Research Establishment Valcartier, Valcartier QUE (CAN)

ABSTRACT: (U) A multiple-scattering lidar equation is derived from a phenomenological representation of the scattering processes. The contributions are separated into the unscattered, singly scattered, and multiply scattered illuminations of the scattering volume, a single backscattering reflection from that volume, and the unscattered and multiply scattered propagation back to the receiver. The equation is obtained in the form of analytic expressions that explicitly show the signal dependence on the extinction coefficient, the effective particle size, the range, and the receiver field of view. Consistent agreement is found with Monte Carlo calculations and published laboratory measurements. Numerical simulations demonstrate that measurements made at three or more fields of view can be inverted to solve for the extinction coefficient and the effective particle radius. The multiple scatterings taken into account in the proposed equation are the small-angle diffraction scatterings, the wide-angle scatterings caused by refraction and reflection are considered lost, except for one backscattering at an angle close to 180 degrees. Consequently, the equation is applicable to cases in which the projection of the lidar receiver field of view on the cloud is of the order of the angular width of the diffraction peak of the phase function times the penetration depth into the cloud.
DESCRIPTORS: (U) LIDAR;Scattering;Algorithms;Aerosols;Clouds (meteorology);Wave propagation;Atmospheric attenuation;Particle size;Optical radar
IDENTIFIERS: (U) Laser radar;Extinction coefficients;Field of view;Lidar inversion

REPORT DATE: 20 Nov 1996 **NUMBER OF PAGES :** 17

Reprints: Applied Optics, vol 35, no 33, 1996, p 6449-6465

DRDKIM N°: 97-00232 **CANDIS N°:** 500609 **Format(s):**Hardcopy;Document Image stored on Optical Disk

Date modified: 2003-04-17 Important Notices